48th AIAA Aerospace Sciences Meeting Including the New Horizons Forum and Aerospace Exposition
4 - 7 January 2010, Orlando, Florida
AIAA 2010-437

Aerodynamic Design of an Aircraft-Mounted Pod for Improved Aero-Optic Performance

R. Mark Rennie[1], Grady Crahan[2], and Eric J. Jumper[3]
Center for Flow Physics and Control
University of Notre Dame, Notre Dame, IN, 46556

A new approach for the shaping of pods and fairings for optical systems is presented in which the objective of the approach is to prevent or mitigate aero-optic effects. Basic streamlined shapes are developed which prevent supersonic flow and shock formation around the optical aperture. Furthermore, an innovative design for the shaping of cutouts that extend the maximum aft lookback angle of the optical system is described. The design approach is supported by computational fluid dynamic analyses, and the design of planned wind-tunnel tests is presented.

Nomenclature

C_P	=	pressure coefficient
C_{P0}	=	pressure coefficient in incompressible flow
D	=	turret ball diameter
M	=	Mach number
r	=	radial coordinate
x	=	axial coordinate
ϕ	=	azimuthal angle
θ	=	elevation angle

I. Introduction

AN aircraft traveling at compressible flow speeds is surrounded by optically-active regions associated with compressible turbulent flows. These optically-active flow regions can have disastrous consequences for a beam of light that traverses the region, thereby restricting the effective field of regard of an optical system carried by the aircraft. The study of the optical character of high-speed turbulent flows, such as boundary layers [1] or shear layers [2] is called "aero-optics." Flow-induced optical aberrations can also be produced, however, by inviscid flows such as shock waves.

A possible mitigation approach to aero-optic flows is to employ an adaptive-optic (AO) system [3] that places the conjugate waveform of the aberration onto the wavefront of the beam prior to its transmission through the aberrating flowfield. Due to the inability of contemporary AO systems to match the high temporal frequencies associated with aero-optic flows, feedforward approaches are under development [4] that employ flow-control techniques to pre-condition critical regions of the flow thereby increasing the effective bandwidth of the AO system. The difficulties associated with AO approaches suggest, however, that considerable advantage could be gained by careful aerodynamic design of the mounting arrangement for the optical system that avoids the formation of strongly-aberrating flow regions in the first place. This paper details an investigation into the aerodynamic design of airborne optical systems that are specifically intended to prevent or mitigate degradation of the beam due to aero-optic effects. In particular, the paper deals with the design of a pod that could be mounted externally to an aircraft; however, the techniques developed are generally applicable to the design of subsonic, compressible-flow airborne optical systems.

[1]Research Assistant Professor, Department of Aerospace and Mechanical Engineering, Senior Member AIAA.
[2]Graduate Research Assistant, Department of Aerospace and Mechanical Engineering, Student Member AIAA.
[3]Professor, Department of Aerospace and Mechanical Engineering, Fellow AIAA.

II. Design of an Aero-Optic Pod

A. Design Objectives

Probably the simplest and most flexible method of providing control over the aiming direction of an optical system is to mount the system in a spherical turret. Examples of systems employing spherical-turret mounts can be found in [5, 6] and investigations into the aero-optic environment around spherical turrets can be found in [7-9].

In inviscid, incompressible flow, the peak negative C_{P0} on a sphere is -1.25 [10]. In [9], an experimentally-measured minimum C_{P0} of approximately -1.25, corrected to incompressible-flow conditions, was also reported for a hemispherical turret on a D/3 cylindrical base. These C_{P0} values can be corrected for compressibility effects using, for example, the Karman-Tsien correction:

$$C_P = \frac{C_{P0}}{\sqrt{1-M_\infty^2} + \left(\frac{M_\infty^2}{1+\sqrt{1-M_\infty^2}}\right)\frac{C_{P0}}{2}} \tag{1}$$

Similarly, the critical Mach number is given by:

$$C_{Pcrit} = \frac{2}{\gamma M_{crit}^2}\left[\left(\frac{1+\frac{\gamma-1}{2}M_{crit}^2}{1+\frac{\gamma-1}{2}}\right)^{\frac{\gamma}{\gamma-1}} - 1\right] \tag{2}$$

The intersection of these two curves, Fig. 1, shows that supersonic flow and formation of a shock wave occurs on a spherical turret at a Mach number just below M=0.55; this Mach number is significantly below the nominal M≈0.8 cruise speed of jet transports and combat aircraft. Formation of a shock wave around the top of the turret would not only present a catastrophic aberration in itself, but would also very likely induce flow separation and formation of an optically-active downstream shear layer; together, these effects would seriously degrade the performance of an optical system pointing in the aft direction of the turret field of view. One method of increasing the critical Mach number is to use streamlining to reduce the local surface curvature and flow speeds around the aperture. Figure 1 shows that, in order to avoid shock formation up to M=0.8, the spherical turret must be streamlined such that the local C_{P0} around the aperture is no less than approximately -0.24.

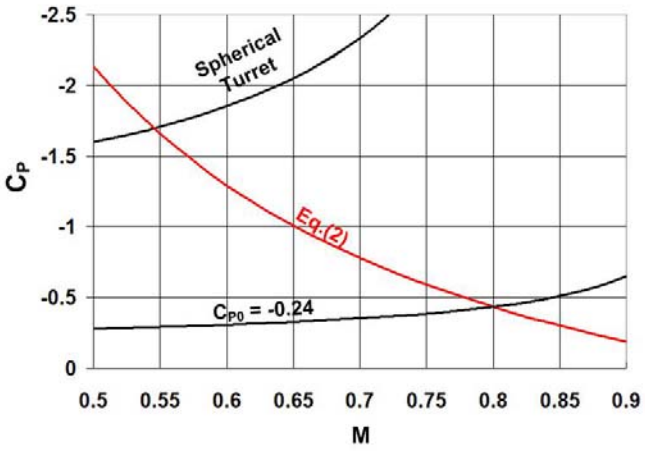

Fig. 1. Critical Mach number for hemisphere and turret [8], and minimum C_P to avoid shock formation during cruise at M=0.8.

Even at flight speeds below the critical Mach number, the aero-optic environment in the aft sector of the turret can still be seriously degraded by flow separation from the rear of the turret which, for a sphere, occurs at an angle of approximately 120° from the direction of the oncoming flow [10]. Figure 2 [8] shows schematically the kinds of flow structures that form in the separated-flow region behind a turret; at compressible flow speeds the shear layer associated with this separated flow region becomes optically active and can seriously degrade the ability to focus an outgoing beam on target in the farfield [4]. In summary, the objectives of the design study were therefore twofold:

- to prevent the formation of supersonic flow regions and associated shock formation around the turret optical aperture,
- to prevent or delay the formation of separated flow regions around the aperture or in areas through which the beam must pass.

B. Basic Pod Shape

Figure 1 shows that, in order to avoid shock formation up to M=0.8, the minimum Cp around the optical aperture must be no less than approximately -0.24; one method of achieving this target is to streamline the spherical turret using an appropriately-shaped fairing. As an example, Fig. 3 shows the aerodynamic fairing mounted behind the spherical optical turret used on the Airborne Laser Laboratory (ALL) [5],

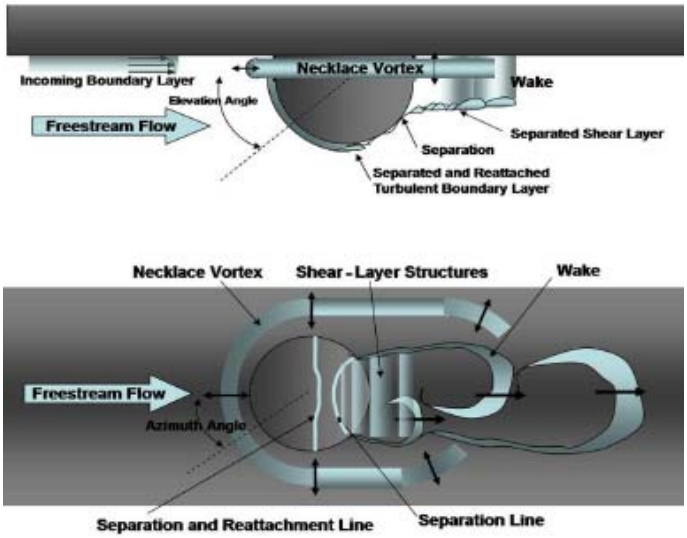

Fig. 2. Flow topology around conformal-window turret [8]

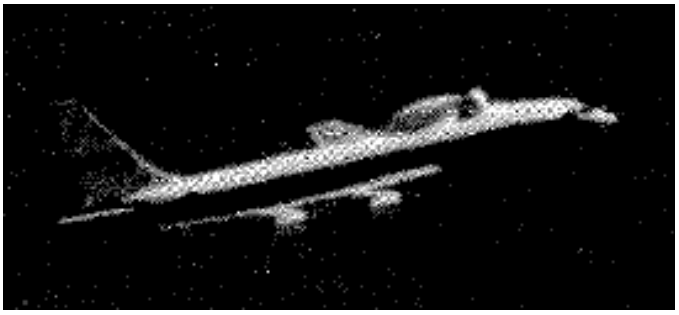

Fig. 3. Example of a fairing applied to a spherical turret mounted on the Airborne Laser Laboratory [5].

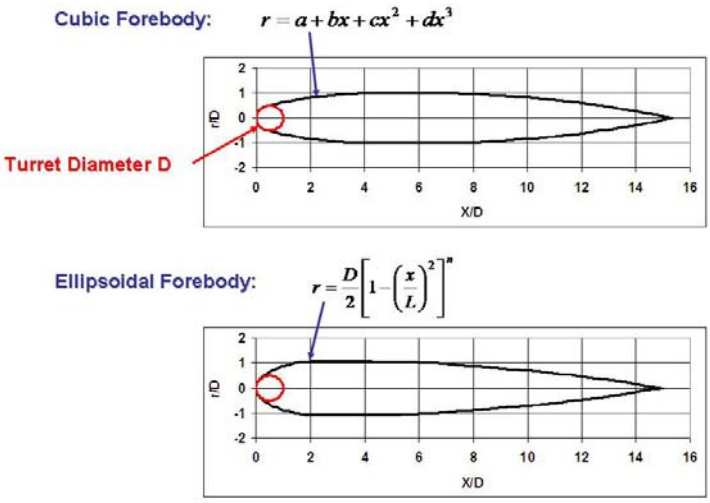

Fig. 4. Examples of pod or fairing shapes that increase the critical Mach number on the turret ball to M=0.8.

indicating that the need for specialized aerodynamic treatment of optical mounts has been recognized for some time.

To eliminate the possibility of shock formation around the optical aperture, the fairing must reduce the surface curvature around the spherical turret so that local flow speeds remain subsonic. A common streamlining shape is the ellipse, given by:

$$r = \frac{D}{2}\left[1 - \left(\frac{x}{L}\right)^2\right] \tag{3}$$

In Eq. (3), r is the radial coordinate of the fairing forebody in a cylindrical coordinate system, and L is the length of the ellipse long axis. Another fairing shape that was tested used a simple cubic to blend the turret ball at the front of the pod with the downstream tail of the fairing; this pod shape was denoted "cubic forebody:"

$$r = a + bx + cx^2 + dx^3 \tag{4}$$

Ellipsoidal and cubic-forebody pod shapes that were found to meet the design objectives are shown in Fig. 4. The shapes are bodies of revolution consisting of a front turret ball and an ogive tail that are blended using the forebody shapes described by Eqs.(3) and (4).

Pressure distributions for the pod shapes were computed using COBALT, which is an unstructured, full Navier-Stokes solver [10]. All of the CFD data presented here were obtained using the inviscid-Euler routines contained in COBALT, since flow separations and other viscous flow effects will be

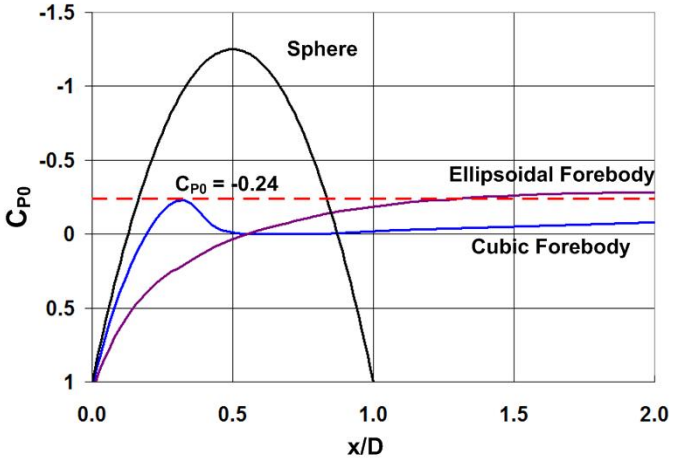

Fig. 5. CFD-computed pressure distributions for basic pod shapes shown in Fig. 4.

determined in wind-tunnel investigation of the most promising pod shapes. The CFD-computed pressure distributions were corrected to "incompressible" flow using Eq. (1). As shown in Fig. 5, both the cubic- and ellipsoidal-forebody shapes shown in Fig. 4 prevent supersonic flow in the vicinity of the turret ball; however, the cubic-forebody shape is thinner, particularly around the front section of the pod, and therefore has some advantage over the ellipsoidal-forebody shape if space constraints are important.

1. Basic Cutout

Based on the preceding results, an isometric sketch of a basic pod shape that is streamlined to prevent shock formation around the aperture is shown in Fig. 6. The pod shape is a simple body of revolution formed from the cubic-forebody shape shown in Fig. 4. The spherical turret ball is located at the front of the pod and can be rotated in elevation and azimuth to point the optical aperture in any direction.

The cubic-forebody shape shown in Fig. 4 contacts the surface of the turret ball at a point that is only approximately 60° past the forward-looking direction. One method of increasing the maximum lookback angle of the pod is to remove a cutout in the pod body immediately downstream of the optical aperture. This cutout would roll with the turret ball around the longitudinal axis of the pod in a rotatable section called a "roll shell." The isometric sketch shown in Fig. 6 includes a cutout and roll shell, and shows how the turret ball would be pointed in elevation and azimuth.

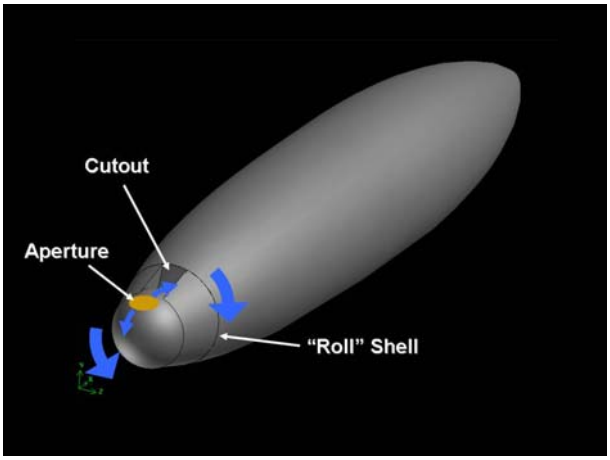

Fig. 6. Basic aero-optic pod layout based on the "cubic-forebody shape, including a basic cutout to enable a greater range of lookback angles.

In Fig. 6, the cutout that enables the aperture to rotate to aft pointing angles has simple, straight walls that are separated by the aperture diameter so that the edges of the aperture will not be obscured by the pod. CFD results show, however, that the critical Mach number for this "simple" cutout design is significantly lower than the M=0.8 target. Part of the cause for this reduction in critical Mach number can be attributed to the fact that the cutout removes some of the streamlining effect of the downstream pod body; however, CFD investigations show that the reduction in critical Mach number can also be attributed to the straight walls of the cutout. As shown schematically in Fig. 7, the flow along the surface of the turret ball normally follows "lines of longitude;" however, the straight walls of the "basic" cutout disrupt this flow pattern by constricting the streamlines over the top of the turret ball, resulting in increased flow speeds over the top of the ball and contributing to the observed reduction in critical Mach number. The straight cutout walls also diffuse the flow on the back of the ball faster than if the flow followed lines of longitude on the ball surface; this higher diffusion increases the adverse pressure gradient on the back of the turret ball thereby increasing the risk of flow separation and associated aero-optic aberrations.

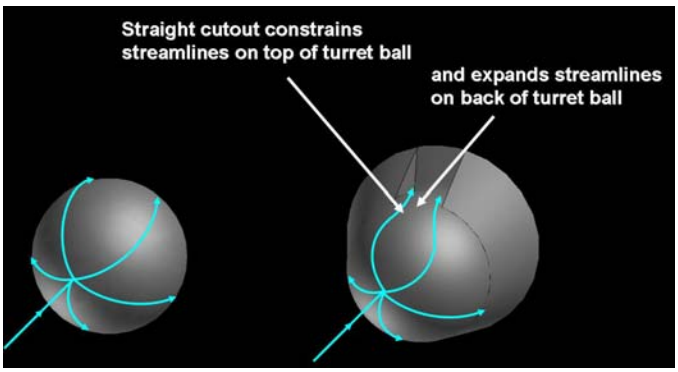

Fig. 7. Illustration showing how straight cutout walls constrain streamlines on the turret ball

2. Improved Cutout

It is apparent from Fig. 7 that the performance of the fairing would be improved if the cutout walls were shaped to follow "lines of longitude" on the surface of the spherical turret ball; however, it is possible to shape the cutout walls to obtain even better performance. Considering the flow between the surface of the turret ball and an undisturbed streamline far from the pod, Fig. 8 shows that the front of the turret ball has the effect of accelerating the flow like a contraction, while the back of the ball decelerates the flow like a diffuser; these effects lead to increased flow speeds around the top of the ball and a reduction in critical Mach number, and reduced flow speeds at the back of the turret ball with an increased chance for flow separation. These effects can be counteracted by shaping the cutout walls to diffuse the flow at the front of the turret ball, and contract at the back of the ball. The effectiveness of the cutout walls can be enhanced by extending the walls into the flow with a "fence."

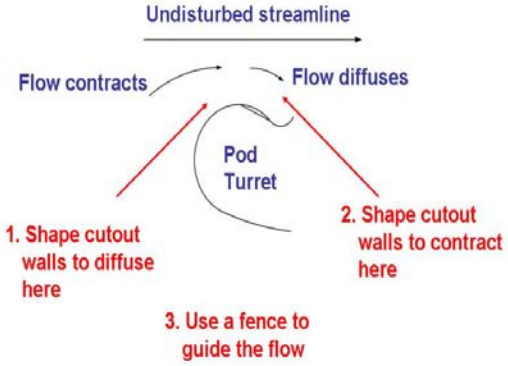

Fig. 8. Schematic showing how cutout shaping can be used to control the local flow around the turret ball.

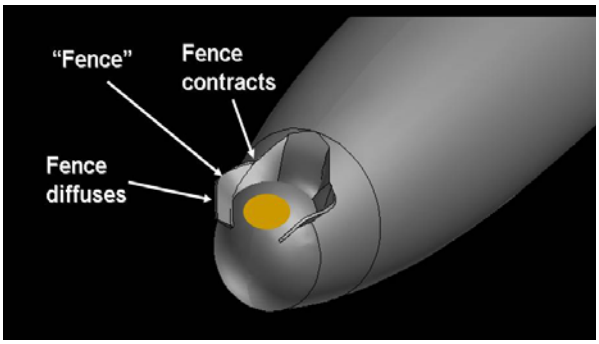

Fig. 9. Pod with improved cutout and fence to control flow around aperture.

An example of a fairing with an improved cutout shape that implements these ideas is shown in Fig. 9. The cutout wall coordinates are determined using fifth-order polynomials for both the contracting and diffusing sections. The use of fith-order polynomials is often used for wind-tunnel contraction design [12]. For the diffuser section, a fifth-order polynomial might be considered overly "aggressive" since it is likely to produce large wall diffusion angles that are prone to boundary-layer separation; however it should be recognized that the flow around the front of the turret ball is still dictated primarily by the ball curvature so that the flow, in fact, still contracts through the upstream "diffusion" section of the fence. Since the walls must "contract" and "diffuse" with respect to lines of longitude on the turret ball surface, the fifth-order polynomials that describe the fence shape were formulated in spherical coordinates:

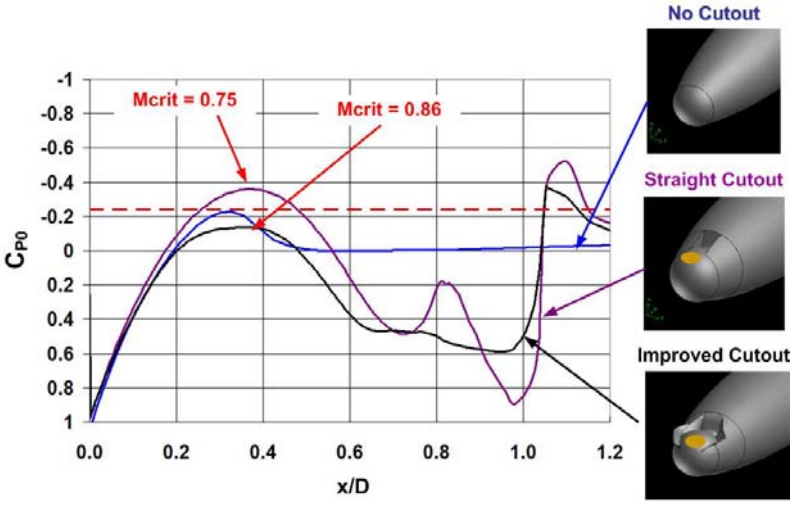

Fig. 10. CFD-computed pressure distributions around turret ball and critical Mach numbers for different cutout configurations. "Straight" and "Improved" Cutout configurations are designed for a maximum lookback angle of 20°

$$\phi_d = aB_d + b_d\theta + c_d\theta^2 + d_d\theta^3 + e_d\theta^4 + f_d\theta^5$$

$$\phi_c = a_c + b_c\theta + c_c\theta^2 + d_c\theta^3 + e_c\theta^4 + f_c\theta^5 \quad (5)$$

where ϕ_d and ϕ_c are the azimuthal location of the cutout wall on the ball surface for the diffusing and contracting sections respectively. The six constants *a, b, c, … f* for each section are determined by the six boundary conditions consisting of the chosen starting and ending azimuthal locations of the fence, plus zero slope and curvature at the start and end of each section of the fence.

Pressure distributions along the centerline of the cutout, computed using CFD for the unmodified pod, the pod

with a simple straight-wall cutout, and a pod with improved cutout are shown in Fig. 10. The figure shows that the critical Mach number for the pod with the improved cutout is even higher than for the unmodified pod shape (M=0.86 versus M=0.8). Further, the adverse pressure gradient on the back of the turret ball has also been reduced, which reduces the possibility for flow separation and associated aero-optic aberrations. As such, this cutout shaping technique opens a host of new possibilities for the pod design, including reducing the pod thickness, increasing the aperture diameter and/or increasing the aperture look-back angle. The technique is also applicable to other turret designs, including simple surface-mounted hemispherical turrets.

3. *Higher Lookback Angles*

The results presented thus far have been for a pod designed to enable a maximum lookback angle of 20° past the zenith angle. Additional studies have been conducted on pods designed for lookback angles of 40° and 60°. The slot contours along the cutout centerline for each of these lookback angles are shown in Fig. 11. The contours were designed assuming an aperture diameter to turret diameter ratio of 1:3, which is a typical geometry for optical turrets [7, 8]; in this case, the downstream edge of the aperture extends approximately an additional 20° past the optical axis of the aperture, making the goal of achieving attached flow over the full extent of the aperture significantly more difficult.

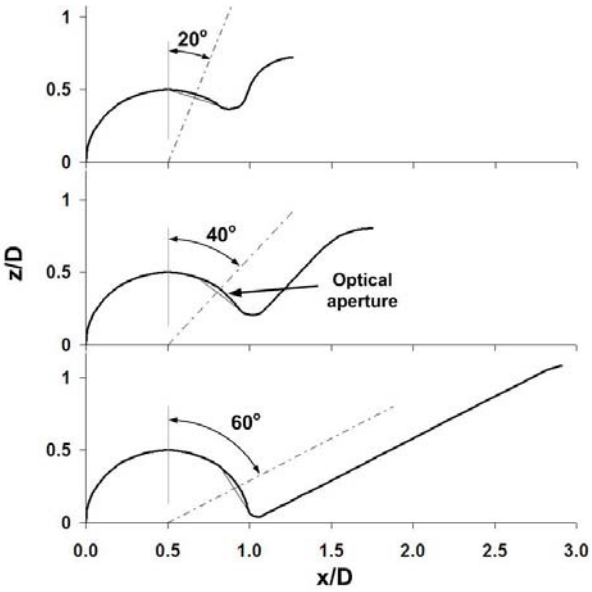

Fig. 11. Contour along cutout centerline for 20°, 40° and 60° lookback angles.

Figures 12 and 13 show pressure distributions over the turret ball for pods with 40° and 60° lookback angles. The figures show that increasing the lookback angle of the pod decreases the minimum pressure on the turret ball and therefore decreases the critical Mach number; this outcome is expected since increasing the lookback angle involves removing more of the downstream fairing so that the beneficial effect that the fairing has on controlling the critical Mach number is reduced. Figures 12 and 13 include, however, C_{P0} distributions for cutouts with the exact same wall shape but with slightly higher fences. The figure shows that increasing the fence height improves the effectiveness of the fence so that, for the 40° lookback case, the M_{CRIT}>0.8 goal can still be achieved using a 20% taller fence. For the 60° lookback case, Fig. 13 shows that the same 20% increase in fence height still leaves the critical Mach number less than M=0.8; in this case an approximately 30% higher fence is required. Further CFD investigations are being conducted to determine successful pod and cutout shapes for lookback angles of 60° and greater; these investigations include looking into modified wall/fence shapes as well as increasing the fence height.

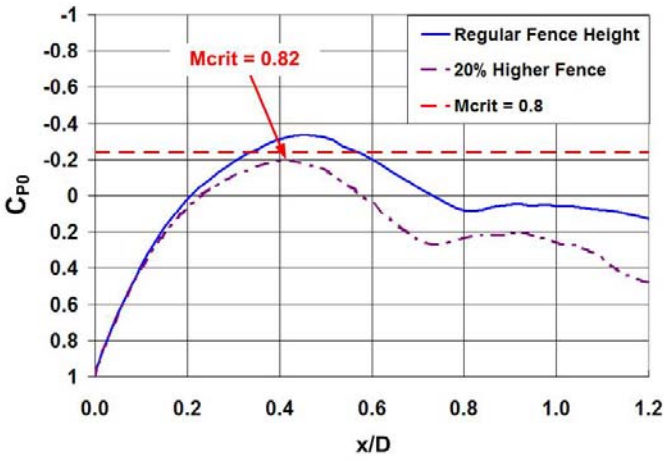

Fig. 12. CFD-computed pressure distributions around turret ball and critical Mach numbers for pod with improved cutout configured for a maximum 40° lookback angle.

4. *Flow Separation*

As discussed above, a second goal of the pod design is to prevent flow separation on the rear of the turret ball. The CFD results presented thus far have all been obtained using an inviscid Euler routine and have concentrated primarily on the prevention of supersonic flows in the vicinity of the turret aperture. An indication of the likelihood of separation can still be obtained, however, by examining the pressure distributions on the rear of the turret from the inviscid Euler computations. Figure 14 compares inviscid-Euler results for the cutout geometries shown in Fig. 11 to experimental measurements on a hemisphere-on-cylindrical-

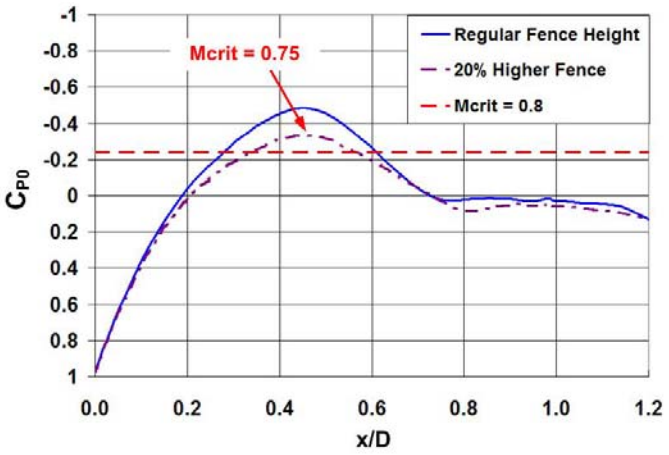

Fig. 13. CFD-computed pressure distributions around turret ball and critical Mach numbers for pod with improved cutout configured for a maximum 60° lookback angle.

base optical turret. The figure shows that the computed adverse pressures on the rear of the turret ball (i.e. from $x/D \sim 0.5$ to 1.0) for all three lookback angles are less severe than the experimentally-measured adverse pressure gradient that precedes flow separation on the turret at $x/D \sim 0.65$; this suggests that the cutout wall shapes used for all three lookback angles could successfully prevent flow separation. Furthermore, the figure shows that the pressures on the rear of the turret ball are actually less severe for the 40° and 60° lookback angles than for the 20° lookback angle; referring to Fig. 11, this result shows that a more gradually-shaped ramp downstream of the turret ball performs better at preventing flow separation on the back of the ball by presenting a more streamlined shape downstream of the turret ball. A full investigation of flow separation around the optical aperture will be conducted in wind-tunnel studies planned for the near future.

C. Wind Tunnel Testing

In addition to the CFD studies described above, wind-tunnel investigations are being planned to test the pod shapes and cutout designs described thus far. The objectives of the wind-tunnel investigations are to:

- verify the CFD results,
- check for boundary-layer separation and shear-layer formation on the back of the turret ball,
- acquire optical data with the pod.

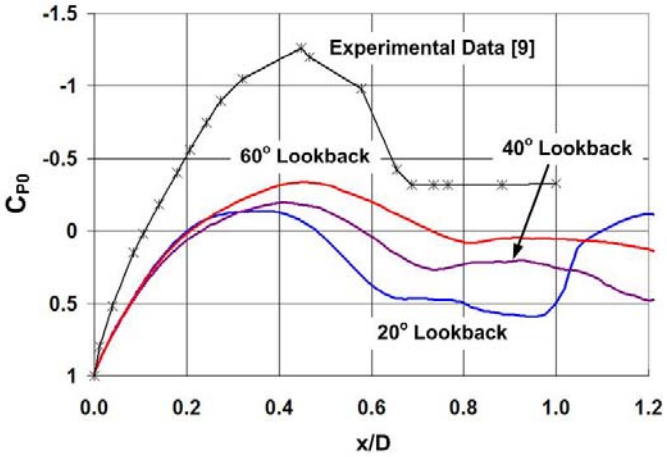

Fig. 14. Comparison of CFD-computed pressure distributions for the cutouts shown in Fig. 11 to experimental data for a hemisphere-on-cylinder turret [8].

The first two objectives can be accomplished by low-speed pressure-measurement and flow-visualization studies and will be conducted in one of the low-speed wind tunnels at the University of Notre Dame. These wind tunnels have 2 ft x 2ft square test sections and a maximum wind speed of approximately 30 m/s (100 ft/s). The pod model will have a modular layout so that different configurations can be tested with different fence shapes and lookback angles. CFD studies have shown that accurate flow around the turret ball can still be achieved if only the top half of the pod is modeled; as such the wind-tunnel pod model will be a half-model which will be mounted on a ground plane. To keep wind-tunnel blockage within acceptable bounds, the pod model will be scaled around a 6-inch diameter turret ball. For the low-speed wind-tunnel investigations, boundary-layer trip devices will be installed on the turret ball to better simulate high-Reynolds-number flows; this boundary-layer control technique has been successfully performed using a 6-inch spherical turret in other investigations conducted at Notre Dame. A drawing of the pod wind-tunnel model is shown in Fig. 15. A schematic of the test layout in a 2 ft x 2ft wind tunnel is shown in Fig. 16.

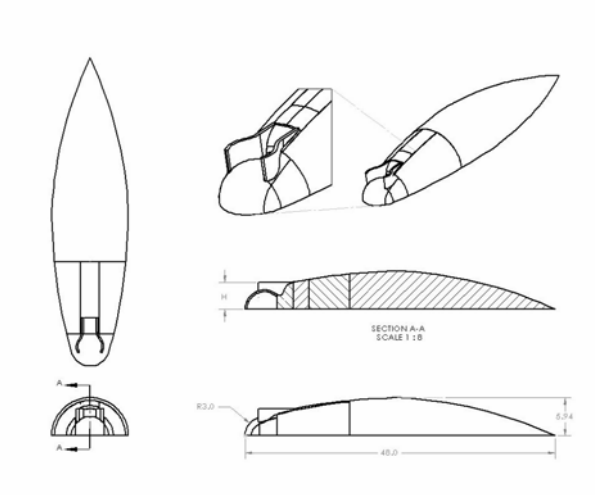

Fig. 15. **Drawing of pod model for wind-tunnel tests.**

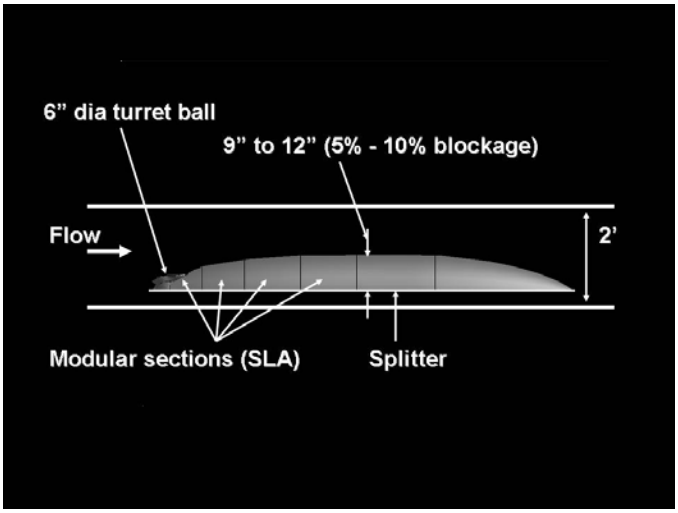

Fig. 16. **Schematic of wind-tunnel test layout.**

Optical measurements are also anticipated using the pod model; these measurements will be performed in Notre Dame's high-speed, M=0.6 capable, 3 ft x 3ft tunnel. For these optical measurements, a 6-inch diameter optical turret will be manufactured, and wavefront measurements will be made at different elevation angles to evaluate the effectiveness of the pod and fairing designs.

Acknowledgments

These efforts were sponsored by the Office of Naval Research under Award Number N00014-07-1-0291. The U.S. Government is authorized to reproduce and distribute reprints for governmental purposes notwithstanding any copyright notation thereon.

References

[1] Gordeyev, S., and Jumper, E.J., "Aero-Optical Characteristics of Compressible Subsonic Turbulent Boundary Layers," AIAA-2003-3606, June, 2003.
[2] Rennie, R. M., Siegenthaler, J. P., and Jumper, E. J., "Forcing of a Two-Dimensional, Weakly-Compressible Subsonic Free Shear Layer," AIAA 2006-0561, Jan., 2006.
[3] Tyson, R.K., *Principles of Adaptive Optics*, Academic Press, Inc., San Diego, 1991.
[4] Rennie, R.M., Duffin, D.A., and Jumper, E. J., "Characterization and Aero-Optic Correction of a Forced Two-Dimensional, Weakly-Compressible Subsonic Free Shear Layer," *AIAA Journal*, Vol. 46, No. 11, 2008, pp.2787-2795.
[5] Duffner, R. W., *Airborne Laser, Bullets of Light*, Plenum Press, New York, 1997.
[6] Lamberson, S., Schall, H.B., and Alvarado, O.L., "Overview of Airborne Laser's Test Program," AIAA 2005-650, Dec., 2005.
[7] Gordeyev, S., Hayden, T., and Jumper, E., "Aero-Optical and Flow Measurements Over a Flat-Windowed Turret," *AIAA Journal*, Vol. 45, No. 2, 2007, pp.347-357.
[8] Gordeyev, S., Post, M.L., McLaughlin, T., Ceniceros, J., and Jumper, E.J., "Aero-Optical Environment Around a Conformal-Window Turert," *AIAA Journal*, Vol. 45, No. 7, 2007, pp.1514-1524.
[9] Gordeyev, S. and Jumper, E.J., "Fluid Dynamics and Aero-Optical Environment Around Turrets," AIAA Paper 2009-4224, June, 2009.
[10] White, F.M., *Fluid Mechanics, 3rd Ed.*, McGraw-Hill, New York, 1994.
[11] Strang, W.Z., Tomaro, R.F., and Grismer, M.J., "The Defining Methods of $Cobalt_{60}$: A Parallel, Implicit, Unstructured Euler/Navier-Stokes Flow Solver," AIAA Paper 1999-0786, Jan. 1999.
[12] Saric, W.S., and Reshotko, E., "Review of Flow Quality Issues in Wind Tunnel Testing," AIAA Paper 1998-2613, June, 1998.